Electronic Supplementary Material (ESI) for Nanoscale Horizons.
This journal is © The Royal Society of Chemistry 2018

Electronic Supplementary Information

Anisotropic microfibres of a liquid-crystalline diketopyrrolopyrrole by self-assembly assisted electrospinning

Markus Hecht, Bartolome Soberats, Jian Zhu, Vladimir Stepanenko, Seema Agarwal, Andreas Greiner and Frank Würthner*

* E-mail: wuerthner@uni-wuerzburg.de

Table of contents

1. Materials and methods

Reagents were purchased from commercial suppliers (Sigma-Aldrich, ACROS, Alfa Aesar, Merck) and used as received without further purification. Solvents were distilled and dried by standard procedures. All reactions were carried out under nitrogen atmosphere.

Flash chromatography: Flash chromatography was carried out with a PuriFlash 450 system from *Interchim* with columns containing silica gel from *Interchim* (PF-30SIHP-F0012, PF-30SIHP-F0025, PF- 30SIHP-F0040, PF-25SIHC-F0025 and dry load columns of various sizes that were filled with silica gel 60 M (particle size: 0.040-0.063 mm from *Merck*). Columns were used according to the recommendation from *Interchim*. Used solvents were of HPLC grade purchased from *Fisher scientific*.

Size exclusion chromatography: Size exclusion chromatography was performed with commercial glass columns using Bio-Beads® S-X3 from Bio-Rad as stationary phase.

NMR spectroscopy: ^{1}H and ^{13}C NMR spectra were recorded on a Bruker Avance III 400 spectrometer operating at 400 MHz (^{1}H) or 100 MHz (^{13}C), with the residual protonated solvent used as the internal standard. The chemical shifts are reported in parts per million (ppm). Multiplicities for proton signals are abbreviated as s, d, t and m for singlet, duplet, triplet and multiplet, respectively.

Mass spectrometry: High resolution mass spectra (HRMS) were recorded on an ESI micrOTOF focus spectrometer (Bruker Daltonic GmbH, Germany).

Elemental analysis: Elemental analyses were performed on a CHN 932 analyzer (Leco Instruments GmbH, Mönchengladbach, Germany).

UV-Vis spectroscopy: UV-Vis absorption spectra in solution were recorded using a JASCO V-770 spectrophotometer. The spectra were measured in quartz glass cuvettes using spectroscopic grade solvents. Temperature control was accomplished by JASCO PAC-743R Peltier system. Extinction coefficients were calculated according to Lambert-Beer’s law. The UV-Vis absorption spectrum of the electrospun fibre was recorded with an Axio Imager 2 (Zeiss, Germany) polarizing optical microscope equipped with a cooled CCD spectrometer MCS-CCD PCI (Zeiss, Germany).

Polarizing optical microscopy (POM): The liquid-crystalline materials were examined under an Axio Imager 2 (Zeiss, Germany) polarizing optical microscope equipped with a LTS420+LNP95 heating stage (Linkam, Great Britain).

Differential scanning calorimetry (DSC): Thermal analyses by DSC were performed on a TA instrument DSC Q1000 with a DSC refrigerated cooling system.

FT-IR spectroscopy: Temperature-dependent and polarized FT-IR spectra were recorded with an AIM-8800 infrared microscope connected to a Shimadzu IRAffinity FT-IR spectrometer. Samples were prepared as a thin films on KBr plates (thickness 2 mm), which were placed on a THMS600 heat stage with a Linkam TP94 controller. Polarization dependent FT-IR spectra were measured by using a precision automated polarizer (ZnSe) from PIKE Technologies. This includes the PIKE Technologies Motion Control Unit and AutoPro software.

Wide-angle and Middle-angle X-ray scattering (WAXS, MAXS): Temperature-dependent WAXS and MAXS measurements were performed on a Bruker Nanostar (Detector Vantec2000, Microfocus copper anode X-ray tube Incoatec). Liquid-crystalline samples were prepared by fibre extrusion using a mini-extruder. The measurements were carried out in Mark capillaries (Hilgenberg) that were positioned perpendicular to the incident X-ray beam. WAXS experiments were performed at a sample detector distance of 21 cm, with the detector tilted by 14° upwards in order to study the angular range of $2\Theta = 0.8° - 28°$. Additional MAXS studies were carried out at a distance of 28 cm with a linear assembled detector, covering an angular range of $2\theta = 0.7° - 12°$. The WAXS pattern of **DPP 1** was recorded at a distance of 13 cm. Silver behenate was used as calibration standard for WAXS, MAXS. All X-ray data were processed and evaluated with the program datasqueeze (http://datasqueezesoftware.com/).

Density measurements: For density measurements, a small mass of sample (~0.4 mg) was placed in a vial, which was filled with ethanol, followed by ultrasonication to remove the air bubbles embedded within the sample. The sample sank to the bottom of the vial due to its high density compared with ethanol. Water was then added at ~0.1 g per aliquot to gradually increase the solution density at an interval of at least 20 min to ensure thermal equilibrium of the solution. When the sample was suspended in the middle of the solution, the density of the sample was identical to that of the solution.

Atomic force microscopy (AFM): AFM measurements were performed under ambient conditions using a Bruker Multimode 8 SPM system operating in tapping mode in air. Silica cantilevers (OMCL-AC200TS, Olympus) with a resonance frequency of ~150 kHz and a spring constant of ~10 N m^{-1} were used. Samples were prepared by spin-coating of toluene solutions onto HOPG with 7000-10000 rpm.

Selected area electron diffraction (SAED): SAED patterns were obtained with the FEI Titan 80-300 transmission electron microscope operated at 300 kV.

Electrospinning: The electrospinning experiments were carried out with a home-made machine basically containing a high voltage source, a collector and the solution container (syringe). The electric field was applied between the needle (0.3 mm diameter) of the syringe and the collector. The distance between the needle and the collector was 20 cm. The applied voltage at the positive electrode and the flow rate were adjusted between 0 kV to 30 kV and 0.1 ml/h to 2 ml/h for optimized fibre formation. The applied voltage of 20kV at a flow rate of 0.1 ml/h produced **DPP2** fibres. The negative electrode used in this experiment was grounded.

2. Synthetic procedures

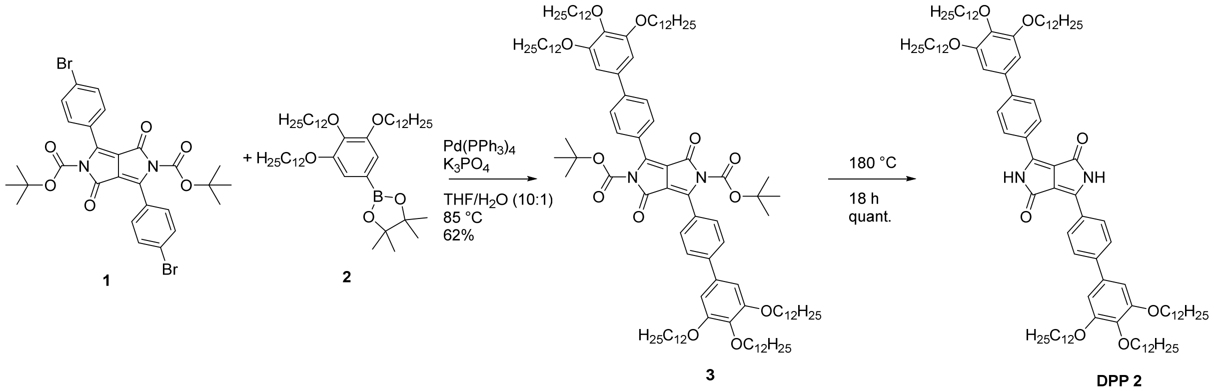

Scheme S1 Synthetic route towards **DPP 2**.

The precursors **1**[1,2] and **2**[3,4] were synthesized according to literature known procedures. The synthesis of **DPP 1** was previously reported by our group.[5]

3,6-Bis(3',4',5'-tris(dodecyloxy)-(1,1'-biphenyl)-4-yl)-2,5-dihydropyrrolo[3,4-*c*]pyrrole-1,4-dione dicarboxylic acid di-*tert*-butyl ester (3)

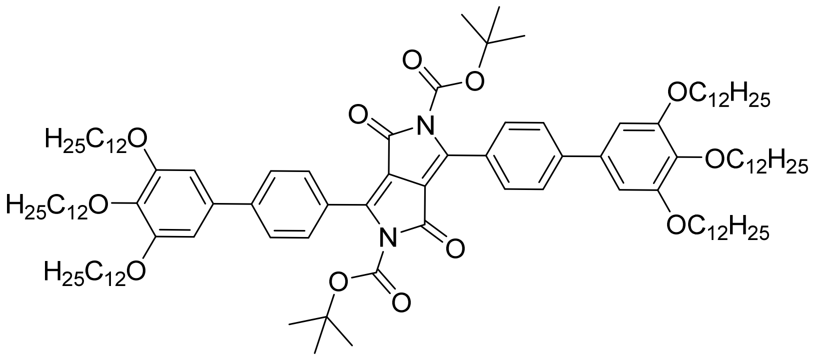

A pressure tube was charged with **1** (211 mg, 0.33 mmol), **2** (586 mg, 0.77 mmol), $Pd(PPh_3)_4$ (52 mg, 45 µmol) and K_3PO_4 (200 mg, 0.94 mmol) under N_2 atmosphere. A mixture of THF and H_2O (10:1) was degassed with N_2 for 1.5 h. The solvent mixture (22 ml) was then added to the pressure tube and the reaction mixture was heated to 85 °C for 5 h. A colour change from bright orange to dark red was observed during the reaction. After being cooled to room temperature, the mixture was diluted with CH_2Cl_2 (150 ml) and water (100 ml). The organic phase was separated and the solvent was removed under reduced pressure. The crude product was purified by flash chromatography (pentane:CH_2Cl_2 1:0 → 7:3) and consecutive size exclusion chromatography (BioBeads SX3, CH_2Cl_2).

Yield: 355 mg (0.20 mmol, 62%) of an orange-red solid.

^{1}H NMR (400 MHz, $CDCl_3$): $\delta = 7.82$ (d, $^3J = 8.6$ Hz, 4H, Ar*H*), 7.66 (d, $^3J = 8.6$ Hz, 4H, Ar*H*) 6.81 (s, 4H, Ar*H*), 4.03 (m, 12H, OCH_2), 1.81 (m, 12H, OCH_2CH_2), 1.54-1.44 (m, 12H, $O(CH_2)_2CH_2$), 1.49 (s, 18H, boc CH_3), 1.40-1.23 (m, 96H, alkyl), 0.87 (m, 18H, CH_3).

^{13}C NMR (100 MHz, $CDCl_3$): $\delta = 159.7$, 153.6, 148.6, 145.9, 144.7, 138.8, 135.3, 129.1, 126.9, 126.8, 112.4, 106.1, 85.5, 73.7, 69.5, 32.1, 30.5, 29.9, 29.8, 29.6, 29.5, 27.8, 26.3, 22.8, 14.3.

HRMS (ESI-TOF, positive mode, MeCN/$CHCl_3$ 1:1): *m/z* calculated for $C_{112}H_{180}N_2O_{12}$ $[M+Na]^+$: 1769.3468; found, 1769.3418.

Elemental analysis calculated (%) for $C_{112}H_{180}N_2O_{12}$ [M = 1746.67 g/mol]: C 77.02 H 10.39 N 1.60; found, C 77.05 H 10.62 N 1.41.

3,6-Bis(3',4',5'-tris(dodecyloxy)-(1,1'-biphenyl)-4-yl)-2,5-dihydropyrrolo[3,4-*c*]pyrrole-1,4-dione (DPP 2)

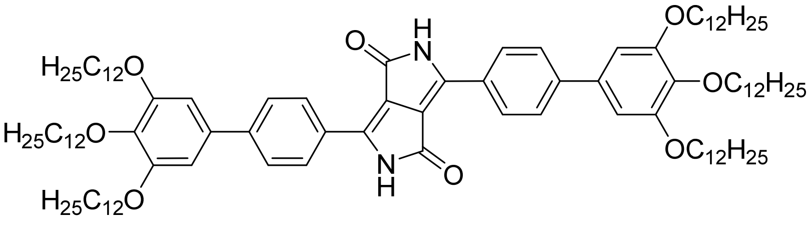

Precursor **3** (211 mg, 0.14 mmol) was dissolved in CH_2Cl_2 (40 ml). The solvent was removed quickly under reduced pressure to form a thin layer of material in the flask. The flask was then heated to 180 °C for 18 h.

Yield: The product is obtained quantitatively as a dark-red wax-like solid.

M.p. 270 °C

^{1}H NMR (400 MHz, $CDCl_3$:DMSO-d_6, 99:1): δ = 10.10 (s, 2H, N*H*), 8.42 (d, ^3J = 8.5 Hz, 4H, Ar*H*), 7.68 (d, ^3J = 8.5 Hz, 4H, Ar*H*), 6.78 (s, 4H, Ar*H*), 3.98 (m, 12H, OCH_2), 1.76 (m, 12H, OCH_2CH_2), 1.44 (m, 12H, $O(CH_2)_2CH_2$), 1.35-1.20 (m, 96H, alkyl), 0.84 (m, 18H, CH_3).

^{13}C NMR (100 MHz, $CDCl_3$/DMSO-d_6 99:1): δ = 163.3, 153.5, 144.2, 143.9, 138.6, 135.3, 128.5, 127.5, 126.7, 111.4, 105.7, 73.6, 69.3, 32.0, 30.4, 29.8, 29.7, 29.5,29.4, 26.2, 22.7, 14.2.

HRMS (ESI-TOF, positive mode, $CHCl_3$/MeOH 1:1 + 0.1% CHOOH): *m/z* calculated for $C_{102}H_{164}N_2O_8$ $[M+H]^+$: 1547.2600, found: 1547.2530.

Elemental analysis calculated (%) for $C_{102}H_{164}N_2O_8$ [M = 1546.44 g/mol]: C 79.22 H 10.69 N 1.81; found, C 79.06 H 10.99 N 1.69.

UV-Vis ($CHCl_3$, c = 30 µM, nm): λ_{max} (ε_{max} M^{-1} cm^{-1}) = 531 (57000).

3. POM and temperature-dependent UV-Vis absorption spectroscopy

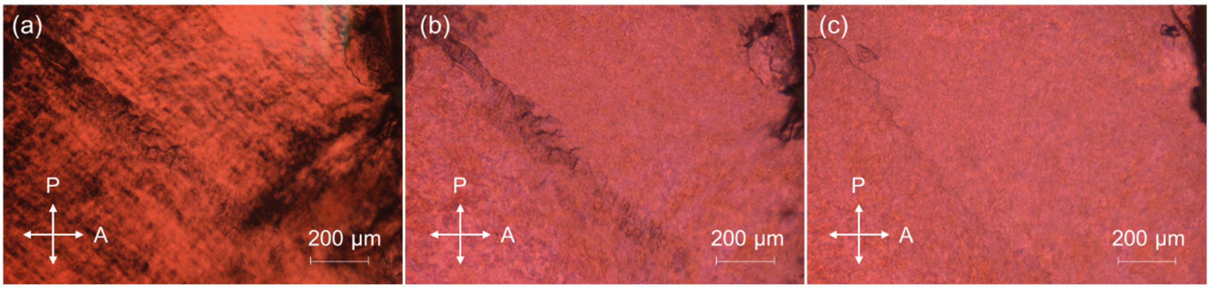

Fig. S1 Polarizing optical microscopy (POM) images of **DPP 2** at (a) 170 °C, (b) 210 °C and (c) 260 °C.

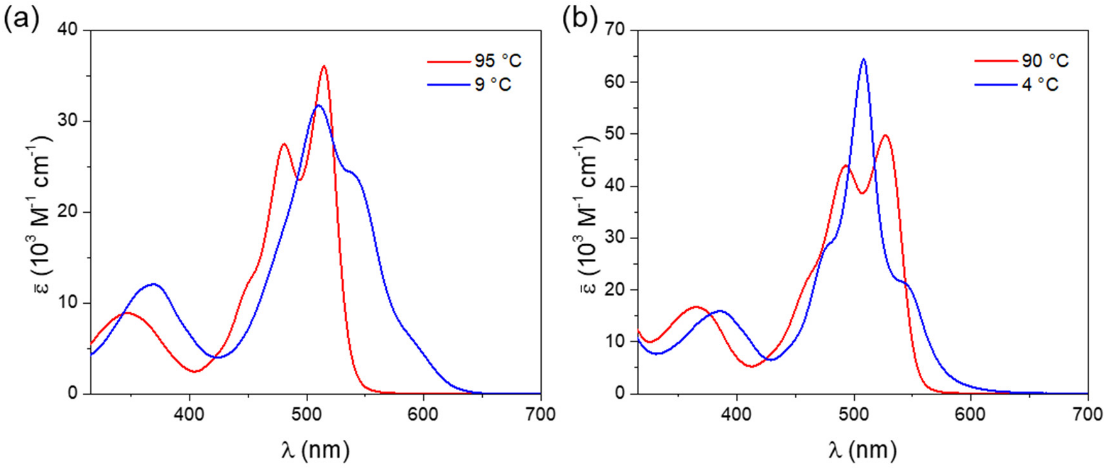

Fig. S2 UV-Vis absorption spectra of (a) **DPP 1** in toluene (c = 4.1 × 10^{-4} M) at 95 °C (red) and 9 °C (blue) and (b) **DPP 2** in toluene (c = 5.0 × 10^{-4} M) at 90 °C (red) and 4 °C (blue).

4. Tube inversion test for gelation

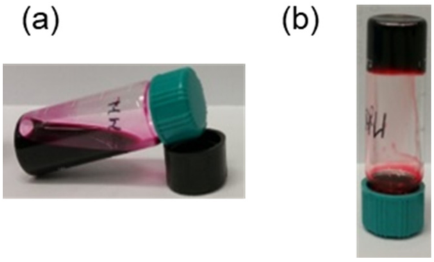

Fig. S3 Tube inversion test of (a) **DPP 1** and (b) **DPP 2** at *c* = 20 mM in toluene.

5. Polarizing optical microscopy of electrospun fibres of DPP 2

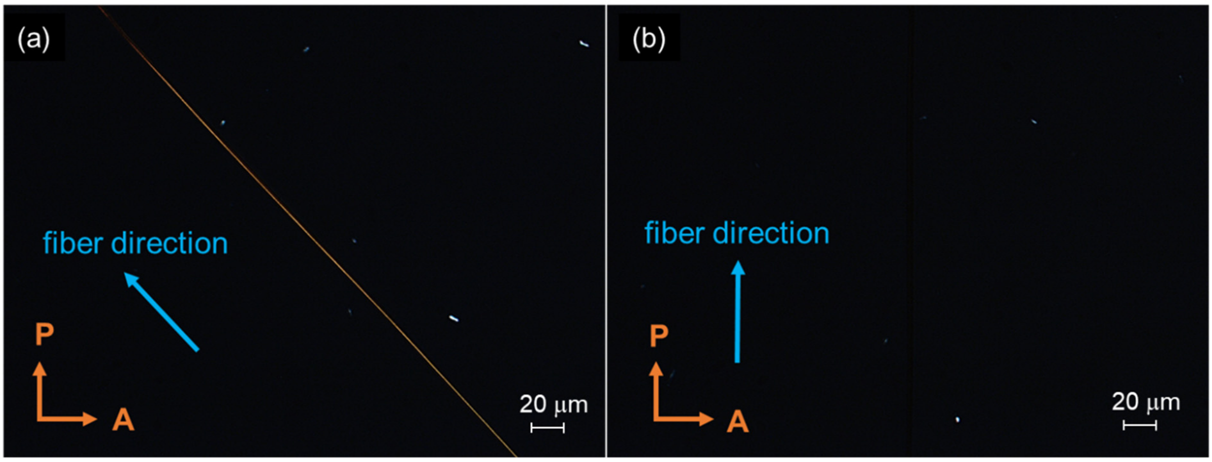

Fig. S4 POM images of an electrospun fibre of **DPP 2** on a glass substrate with the fibre rotated (a) 45° and (b) 0°/90° with respect to the polarizer/analyzer.

In order to probe the anisotropic nature of the electrospun fibres, the sample was investigated with a polarizing optical microscope. Polarizer and analyzer were perpendicular to each other. The microphotographs were captured with the sample oriented in a 45° displacement (Fig. S4a) and along (Fig. S4b) the polarizer and analyzer.

6. Calculated intra- and intermolecular distances

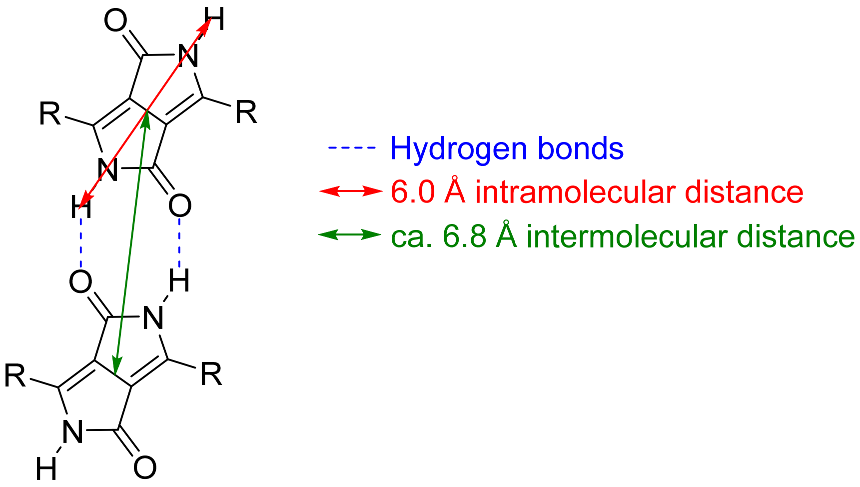

Fig. S5 Schematic illustration of the relevant intra- and intermolecular distances. The structure of the molecule was drawn with ChemDraw and imported to Chem3D. After optimizing the structure in a MM2+ forcefield, the intramolecular distance between NH and NH was calculated to be 6.0 Å. The intermolecular distance represents an estimation of the core to core distance considering the H-bonding distance.

7. Differential scanning calorimetry

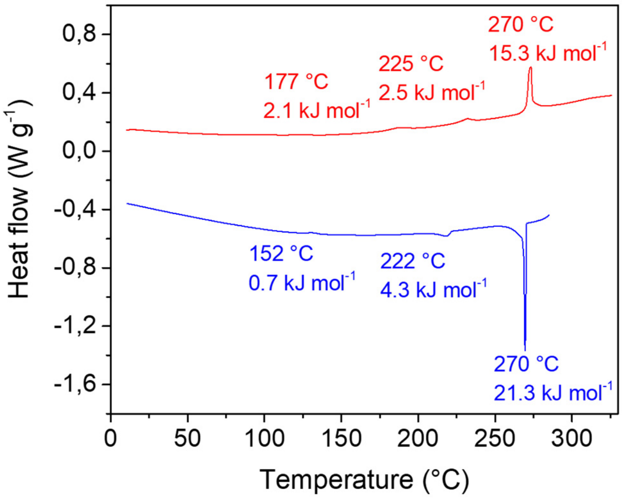

Fig. S6 DSC traces of **DPP 2** in the first cooling (blue) and the second heating (red) process. The heating and cooling rates were 5 °C/min.

8. X-ray scattering

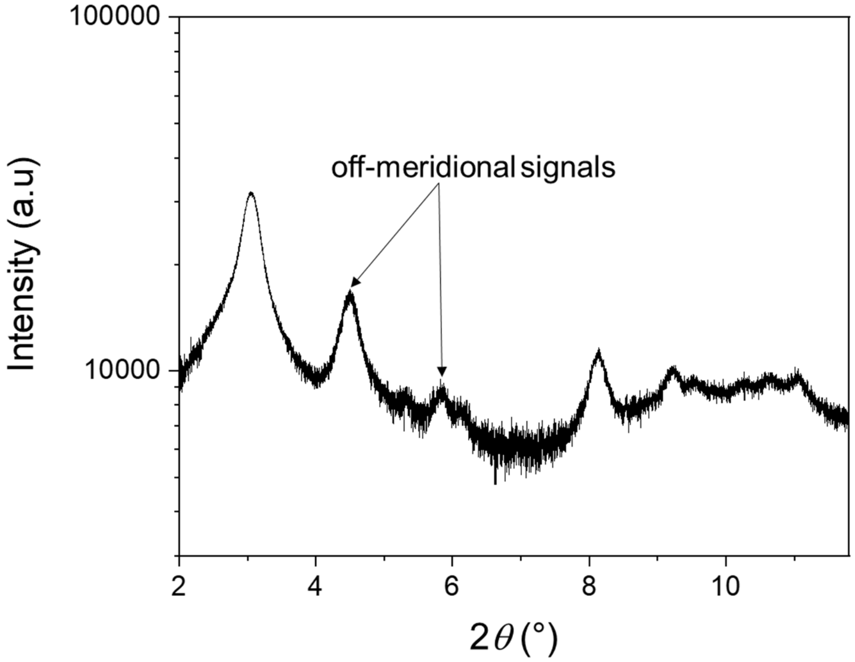

Fig. S7 Integrated intensities along the equator of the WAXS pattern of an aligned fibre of **DPP 2** at 150 °C.

The equatorial signals of the soft crystal (SC) low temperature phase of **DPP 2** could not be unambiguously identified as a columnar hexagonal (a = 33.25 Å) and a columnar centred rectangular (a = 57.85 Å, b = 33.20 Å) unit cell match the experimental signals. Nevertheless, the formation of a columnar unit cell can clearly be seen.

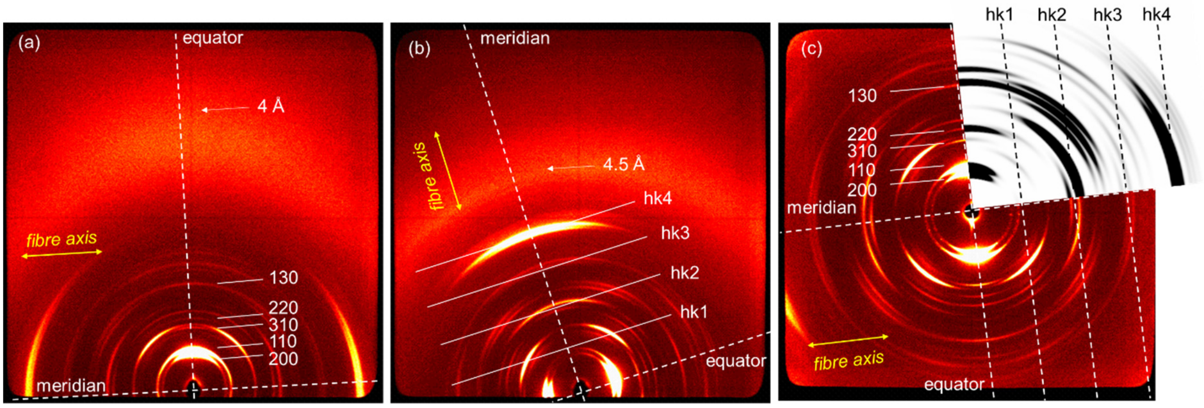

Fig. S8 WAXS patterns of an extruded fibre of **DPP 2** at 210 ˚C with the fibre axis (a) lying and (b) standing. (c) Superposition of the simulated diffraction pattern obtained by CLEARER and the MAXS pattern of **DPP 2** at 210°C.

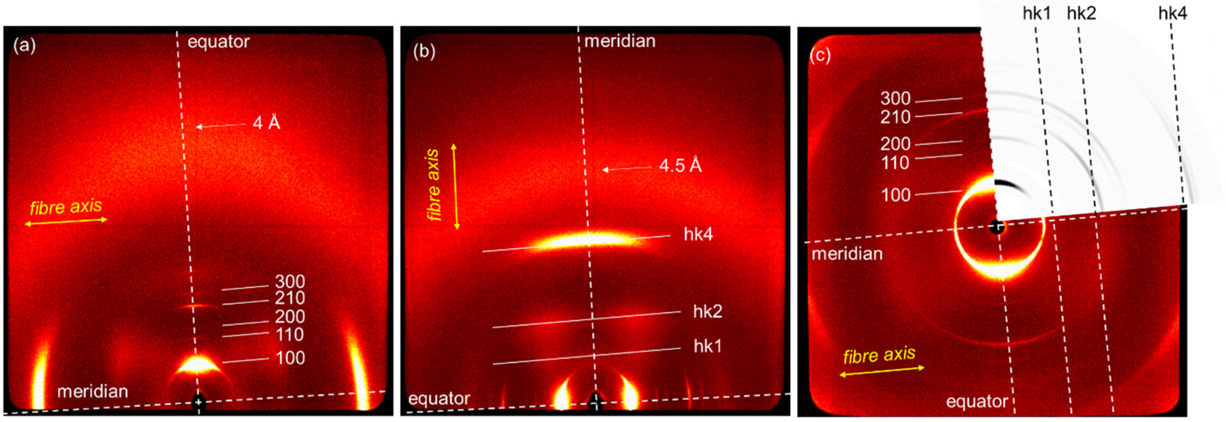

Fig. S9 WAXS patterns of an extruded fibre of **DPP 2** at 265 ˚C with the fibre axis (a) lying and (b) standing. (c) Superposition of the simulated diffraction pattern obtained by CLEARER and the MAXS pattern of **DPP 2** at 265 °C.

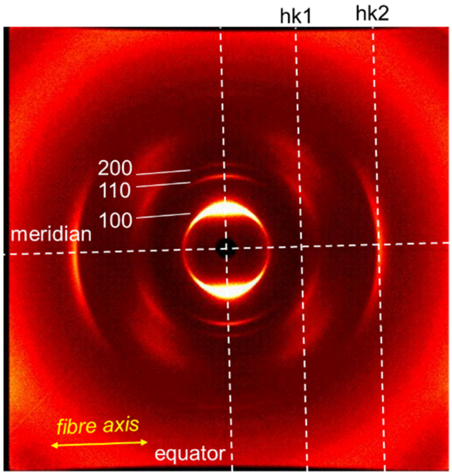

Fig. S10 MAXS pattern of an extruded fibre of **DPP 1** at 80 °C.

9. Polarized FT-IR spectroscopy

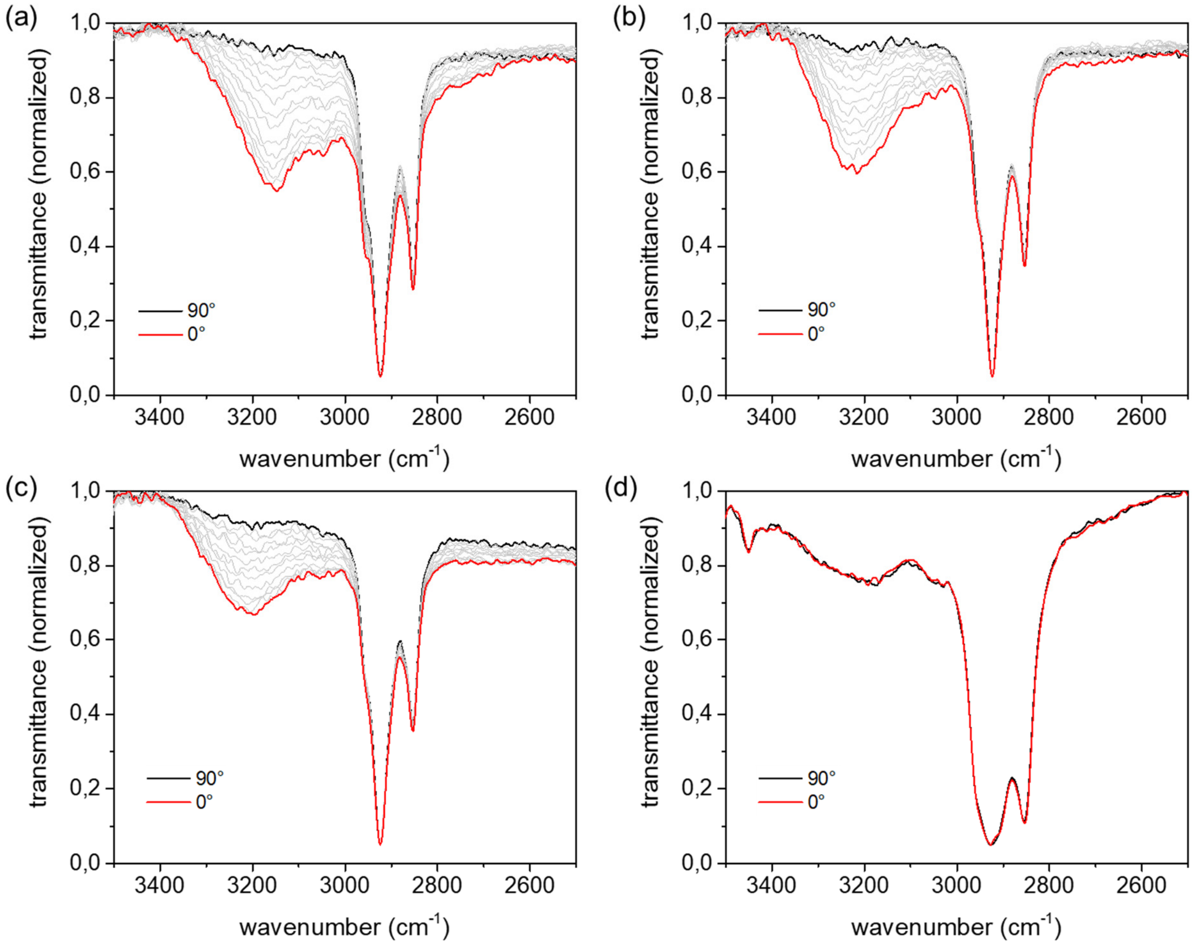

Fig. S11 Polarized FT-IR spectra with different polarization angles of an aligned sample of **DPP 2** at (a) 150 °C (SC), (b) 210 °C (Col$_r$), (c) 250 °C (Col$_h$) and (d) 270 °C (melt). The sample was sheared using an extruded fibre for friction transfer on a KBr substrate. The black line shows the FT-IR spectrum when the polarizer is oriented perpendicular to the shearing direction. The red line shows the spectrum when the polarizer is oriented parallel to the shearing direction.

10. Molecular modelling

The number of molecules Z per columnar stratum was calculated using the following equation:

$$Z = \frac{\delta * N_A * V_{col-strat}}{M}$$

with δ as the density (assumed to be 0.9 g cm^{-3}, adjusted to high temperatures from experimental value), N_A as Avogadro's constant, M as the molecular mass and $V_{col-strat}$ representing the volume of the columnar stratum which was calculated according to

$V_{col-strat} = a^2 * sin60° * h$ for the hexagonal phase

and according to

$V_{col-strat} = a * b * h * 0.5$ for the rectangular phase.

Using the parameters obtained from the X-ray diffraction experiments with a reasonable error margin of 5% per parameter, the number of molecules per columnar stratum was calculated to be 2.10 for the Col_r phase and 2.28 for Col_h phase.[6]

The molecular structure of **DPP 2** with the dodecyloxy substituents being shortened to methoxy groups was geometry optimized using the MM2 forcefield with the program Chem3D. The optimized molecular structure was then imported to *Materials Studio* from BIOVIA.[7] Mirror imaged antiparallel dimers were then built with a distance of 4 Å between the π-cores. The two dimers were then alternately stacked by a rotation of 90° with each dimer. To build the unit cell of the columnar rectangular phase, the structure was placed on the diagonal corners of a rectangular unit cell (a = 65.4 Å, b = 31.5 Å and h = 4 × 6.8 Å = 27.2 Å). The two structures were then moved about *a/4* and *b/4* towards the centre of the unit cell. To build the unit cell of the columnar hexagonal phase, the structure was placed in the centre of a hexagonal unit cell (a = 35.9 Å and h = 4 × 6.8 Å = 27.2 Å). Both model assemblies were then geometry optimized using the force field COMPASS by Ewald summation method, until the non-bonding energy was strongly negative.

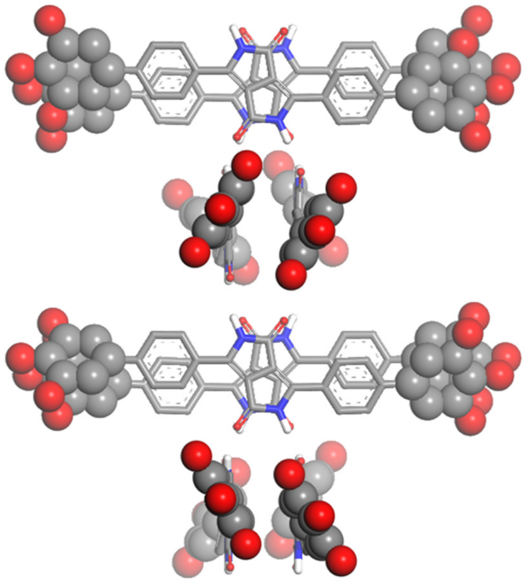

Fig. S12 Model of the geometry optimized unit cell of **DPP 2** for the LC phases (Col$_h$ and Col$_r$) as obtained with *Materials Studio*. The alkyl chains were omitted for clarity. The wedge-shaped substituent is highlighted as CPK model to illustrate the correlation between every fifth molecule induced by the rotationally displaced π-cores.

The fibre diffraction patterns of **DPP 2** were simulated with CLEARER using the geometry optimized structures obtained from *Materials Studio*. The structure was exported as PDB-file and imported into the Fibre Diffraction Simulation module of CLEARER.[8] The fibre axis was set to (0,0,1) with a crystallite size of $a = 100$ nm, $b = 100$ nm and $c = 100$ nm. The fibre disorder parameters σ_Θ and σ_Φ were set to 0.1 radians and infinite, respectively. The sample interval was set to 1 pixel. The contrast was adjusted to best visualize the signals of the pattern.

It needs to be considered that CLEARER simulates the diffraction pattern for a perfectly ordered crystalline domain of a given size on the basis of one unit cell where the disorder of orientation is implemented in the unit cell. Therefore, the intensity of the predicted signals can vary from the experimentally observed ones. However, it should be noted that the relative intensity and the position of the predicted signals are in very good agreement with the ones observed in the experiments.

Fig. S13 Diffraction pattern as simulated with CLEARER for the Col$_r$ phase of **DPP 2**.

Fig. S14 Diffraction pattern as simulated with CLEARER for the Col$_h$ phase of **DPP 2**.

11. UV-Vis experiments

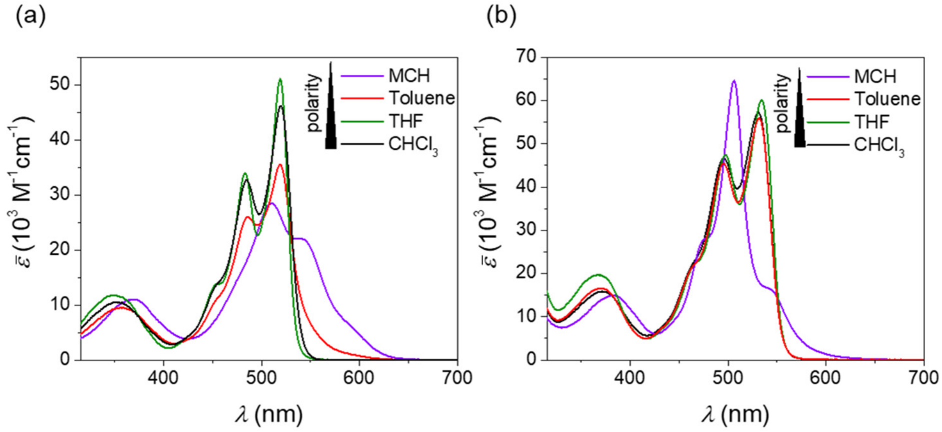

Fig. S15 Solvent-dependent UV-Vis absorption studies of (a) **DPP 1** and (b) **DPP 2** in methyl cyclohexane (MCH, purple), toluene (red), tetrahydrofurane (THF, green) and chloroform (black) at $c = 3.0 \times 10^{-5}$ M.

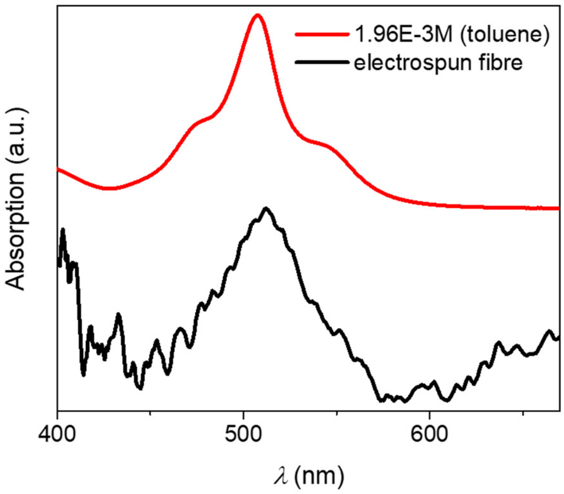

Fig. S16 UV-Vis absorption spectra of **DPP 2** in toluene at $c = 1.96 \times 10^{-3}$ M (red) and of an electrospun fibre of **DPP 2** (black).

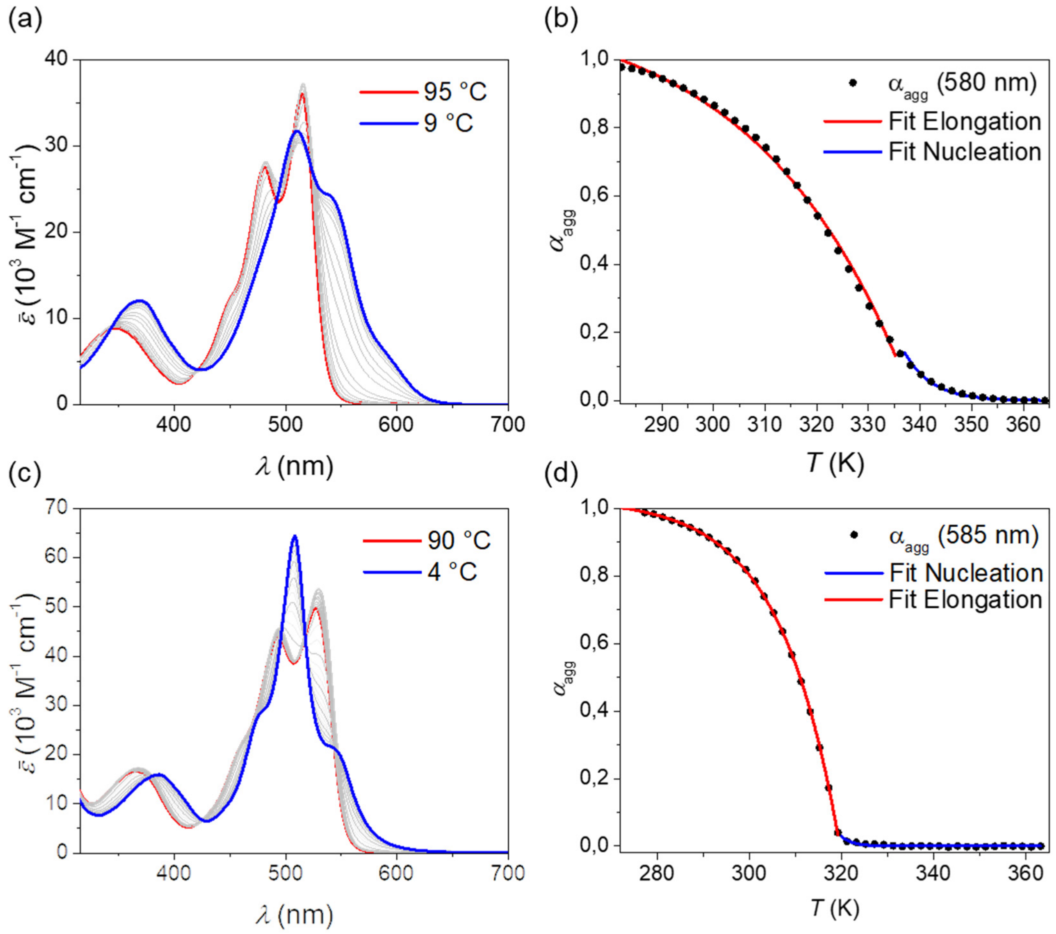

Fig. S17 Temperature-dependent UV-Vis absorption studies of (a) **DPP 1** at $c = 4.1 \times 10^{-4}$ M in toluene and (c) **DPP 2** at $c = 5.0 \times 10^{-4}$ M in toluene and fit according to the cooperative nucleation-elongation model for (b) **DPP 1** at 580 nm and (d) **DPP 2** at 585 nm.

The self-assembly of both compounds was studied by temperature-dependent UV-Vis absorption experiments with heating/cooling rates of 1K/min. The calculated degree of aggregation α_{agg} was fitted according to the cooperative nucleation-elongation model.[9] For **DPP 1**, an enthalpy of $\Delta H = -35$ kJ/mol, an elongation temperature of $T_e = 339$ K and $K_a = 1 \times 10^{-3}$ were obtained for the self-assembly at $c = 4.1 \times 10^{-4}$ M in toluene. For **DPP 2**, an enthalpy of $\Delta H = -65$ kJ/mol, an elongation temperature of $T_e = 320$ K and $K_a = 4 \times 10^{-5}$ were obtained for the self-assembly at $c = 5.0 \times 10^{-4}$ M in toluene.

12. Electrospinning of monomeric solutions

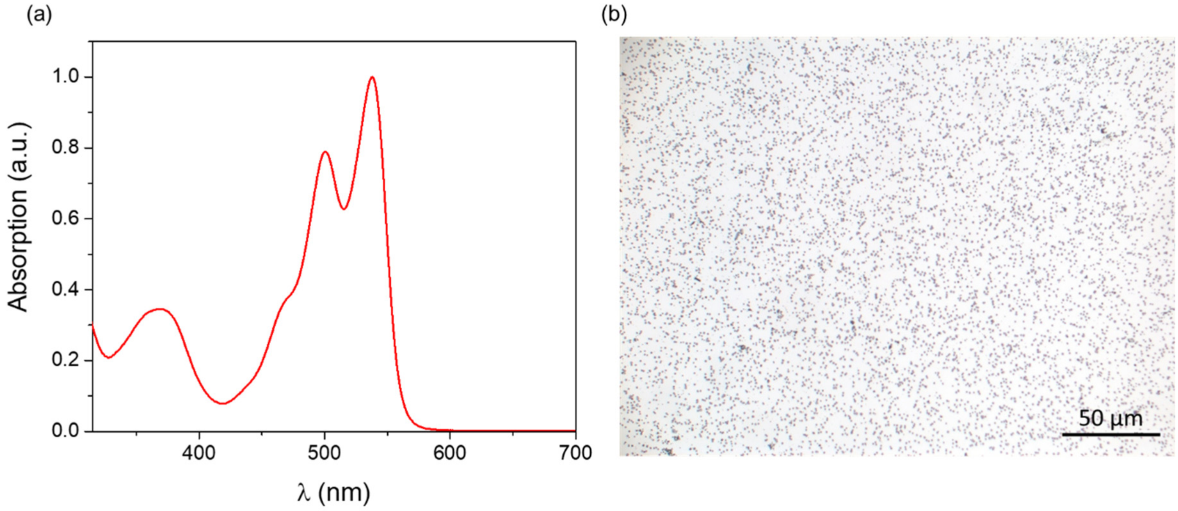

Fig. S18 (a) UV-Vis absorption spectrum of a 20 mM solution of **DPP 2** in toluene/DMF (3/1) showing the characteristic features of monomeric DPP. (b) Microscopic image of the droplets collected from the electrospinning trials of a 20 mM solution of **DPP 2** in toluene/DMF (3/1).

13. NMR spectra of 3 and DPP 2

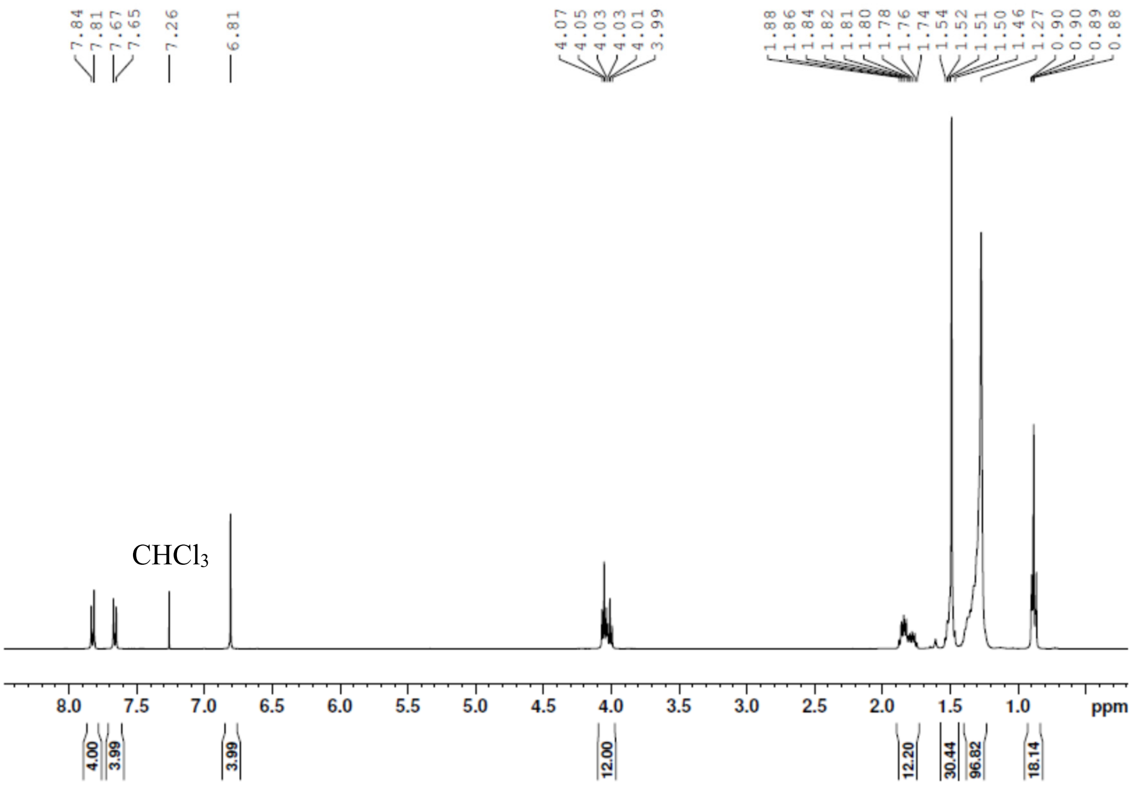

Fig. S19 ^{1}H NMR spectrum (400 MHz) of **3** in $CDCl_3$ at 298 K.

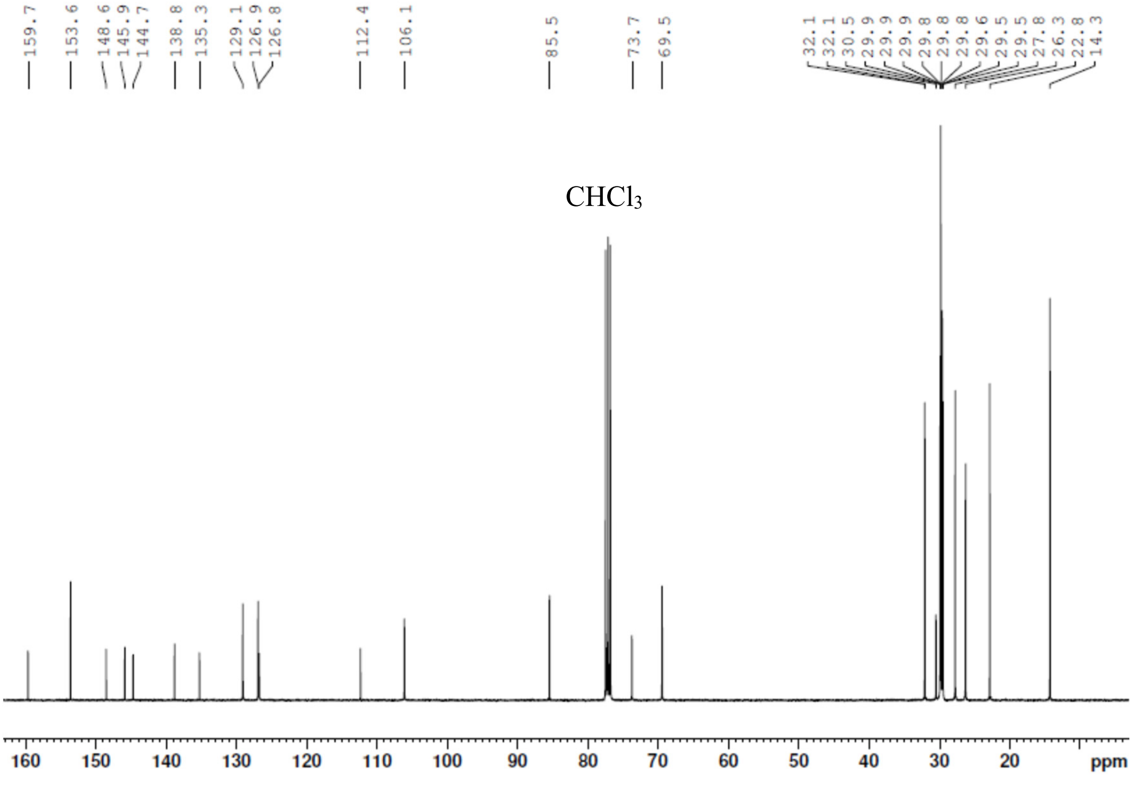

Fig. S20 ^{13}C NMR spectrum (100 MHz) of **3** in $CDCl_3$ at 298 K.

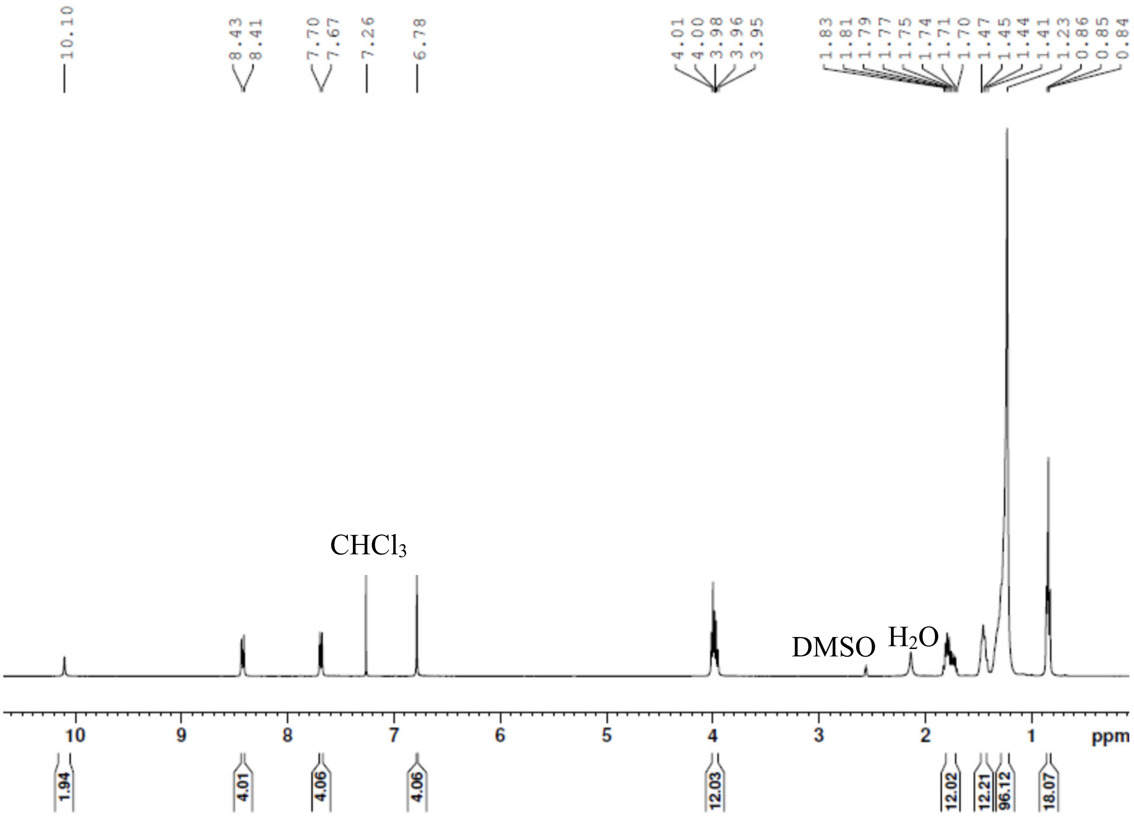

Fig. S21 ^{1}H NMR spectrum (400 MHz) of **DPP 2** in $CDCl_3$:DMSO-d_6 (99:1) at 298 K.

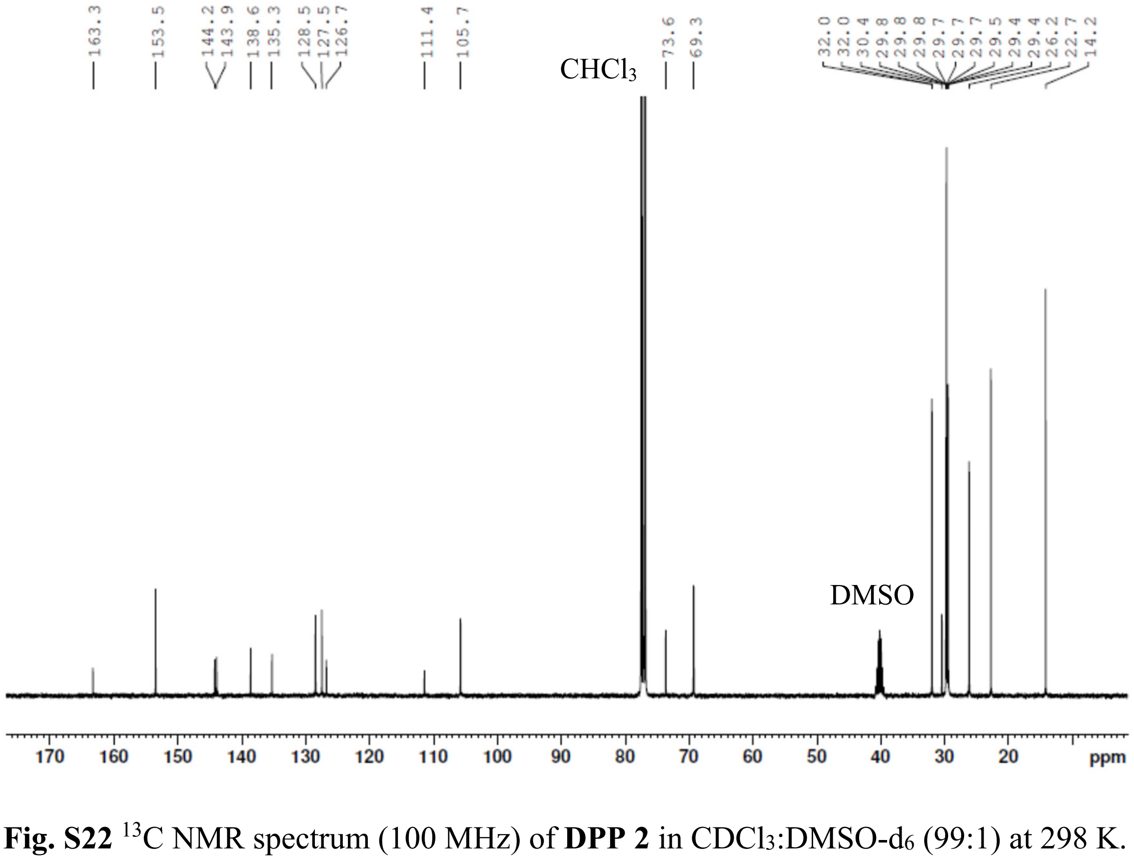

Fig. S22 ^{13}C NMR spectrum (100 MHz) of **DPP 2** in $CDCl_3$:DMSO-d_6 (99:1) at 298 K.

14. References

1 Y.-H. Jeong, C.-H. Lee and W.-D. Jang, *Chem. Asian J.*, 2012, **7**, 1562-1566.

2 M. Fukuda, K. Kodama, H. Yamamoto and K. Mito, *Dyes Pigm.*, 2004, **63**, 115-125.

3 W.-S. Li, Y. Yamamoto, T. Fukushima, A. Saeki, S. Seki, S. Tagawa, H. Masunaga, S. Sasaki, M. Takata and T. Aida, *J. Am. Chem. Soc.*, 2008, **130**, 8886-8887.

4 H. Maeda, K. Chigusa, T. Sakurai, K. Ohta, S. Uemura and S. Seki, *Chem. Eur. J.*, 2013, **19**, 9224-9233.

5 B. Soberats, M. Hecht and F. Würthner, *Angew. Chem. Int. Ed.*, 2017, **56**, 10771-10774.

6 D. Sahoo, M. Peterca, E. Aqad, B. E. Partridge, P. A. Heiney, R. Graf, H. W. Spiess, X. Zeng and V. Percec, *J. Am. Chem. Soc.*, 2016, **138**, 14798-14807.

7 Materials Studio 2017 (7.1.0.48), Dassault Systèmes BIOVIA, San Diego, 2017.

8 O. Sumner Makin, P. Sikorski and L. C. Serpell, *J. Appl. Crystallogr.*, 2007, **40**, 966–972.

9 (a) M. M. Smulders, M. M. Nieuwenhuizen, T. F. de Greef, P. van der Schoot, A. P. Schenning and E. W. Meijer, *Chem. Eur. J.*, 2010, **16**, 362-367; (b) M. M. Smulders, A. P. Schenning and E. W. Meijer, *J. Am. Chem. Soc.*, 2008, **130**, 606-611; (c) T. F. A. De Greef, M. M. J. Smulders, M. Wolffs, A. P. H. J. Schenning, R. P. Sijbesma and E. W. Meijer, *Chem. Rev.*, 2009, **109**, 5687-5754.